Maximization of the connectivity repertoire as a statistical principle governing the shapes of dendritic arbors

Quan Wen[a,1], Armen Stepanyants[b], Guy N. Elston[c], Alexander Y. Grosberg[d], and Dmitri B. Chklovskii[a,2]

[a]Janelia Farm Research Campus, Howard Hughes Medical Institute, 19700 Helix Drive, Ashburn, VA 20147; [b]Department of Physics and Center for Interdisciplinary Research on Complex Systems, Northeastern University, 110 Forsyth Street, Boston, MA 02115; [c]Centre for Cognitive Neuroscience, Sunshine Coast, Queensland 4562, Australia; and [d]Department of Physics, New York University, New York, NY 10003

Edited by Charles F. Stevens, The Salk Institute for Biological Studies, La Jolla, CA, and approved May 21, 2009 (received for review February 11, 2009)

The shapes of dendritic arbors are fascinating and important, yet the principles underlying these complex and diverse structures remain unclear. Here, we analyzed basal dendritic arbors of 2,171 pyramidal neurons sampled from mammalian brains and discovered 3 statistical properties: the dendritic arbor size scales with the total dendritic length, the spatial correlation of dendritic branches within an arbor has a universal functional form, and small parts of an arbor are self-similar. We proposed that these properties result from maximizing the repertoire of possible connectivity patterns between dendrites and surrounding axons while keeping the cost of dendrites low. We solved this optimization problem by drawing an analogy with maximization of the entropy for a given energy in statistical physics. The solution is consistent with the above observations and predicts scaling relations that can be tested experimentally. In addition, our theory explains why dendritic branches of pyramidal cells are distributed more sparsely than those of Purkinje cells. Our results represent a step toward a unifying view of the relationship between neuronal morphology and function.

optimization | scaling | entropy | pyramidal cell | axons

Mammalian neurons consist of a cell body and dendritic and axonal arbors (ref. 1 and Fig. 1). The dendritic arbor is a complex branching structure, which receives signals from thousands of other neurons and conducts them toward the cell body, where they are integrated. The axonal arbor typically spans a larger territory than a dendritic arbor and conducts signals from the cell body to synapses, where signals are transmitted to dendrites of thousands of other neurons (Fig. 1). The majority of synapses on neurons discussed below are formed on short dendritic protrusions called spines (Fig. 1). Because synaptic transmission requires a physical contact between dendrites and axons, dendritic arbor shape determines which axons are accessible to which dendrites (2–9). This suggests that the spatial distribution of dendrites is important for understanding brain function (10–15).

Interestingly, dendritic arbor shape can vary widely among neurons of the same class and between different classes. Consider, for example, pyramidal cells, which comprise ≈80% of all neurons in the cerebral cortex (16). The total length of basal dendrites of pyramidal cells L, and the basal arbor radius R, defined as the rms distance between any 2 dendritic segments (Fig. 2*A*), vary widely among different areas of the cortex (17–19). Furthermore, dendritic branches of pyramidal cells are distributed more sparsely than those of Purkinje cells, the principal neurons in the cerebellum (ref. 11 and Fig. 2*B*). To use these observations for inferring neuronal function, we need to identify principles governing arbor shape.

We start by showing that, within pyramidal cell class, R and L, and the short-range correlation in the locations of dendrites within a cell, follow scaling laws. The corresponding exponents are related, suggesting that statistics of different arbors and different parts of the same arbor are governed by one principle. Second, we propose an explanation for these observations by viewing dendritic arbor shape as an outcome of optimization by natural selection (1), a process that maximizes dendritic functionality for a given dendritic cost to the organism (1, 20–24). Our solution of this optimization problem is consistent with our measurements and accounts for the variation in arbor shape.

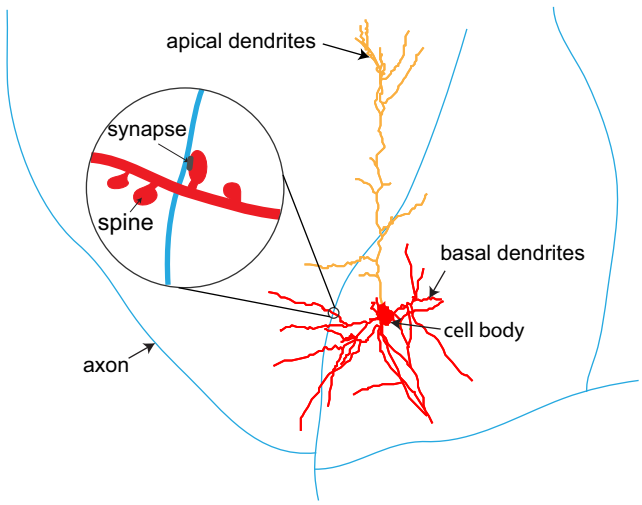

Fig. 1. Schematic illustration of pyramidal cell morphology. Basal dendritic arbor consists of a few primary branches stemming from the cell body and bifurcating repeatedly (red). Apical dendritic arbor (orange) typically consists of a single trunk, which branches in the upper layers of the neocortex. Dendrites receive synapses from axons (blue) of other neurons. These synapses are typically formed on dendritic spines (*Inset*).

Results

Scaling, Universality, and Self-Similarity of Basal Dendritic Arbors of Pyramidal Neurons. We measured dimensions of dendritic arbors from a dataset obtained over the past decade by labeling and

Author contributions: Q.W., A.S., A.Y.G., and D.B.C. designed research; Q.W., A.S., G.N.E., A.Y.G., and D.B.C. performed research; Q.W., A.S., A.Y.G., and D.B.C. analyzed data; and Q.W., A.S., G.N.E., A.Y.G., and D.B.C. wrote the paper.

The authors declare no conflict of interest.

This article is a PNAS Direct Submission.

Freely available online through the PNAS open access option.

Data deposition: The data reported in this paper have been deposited at http://research.janelia.org/Chklovskii/data.htm.

[1]Present address: Department of Physics, Harvard University, 17 Oxford Street, Cambridge, MA 02138.

[2]To whom correspondence should be addressed. E-mail: mitya@janelia.hhmi.org.

This article contains supporting information online at www.pnas.org/cgi/content/full/0901530106/DCSupplemental.

www.pnas.org/cgi/doi/10.1073/pnas.0901530106

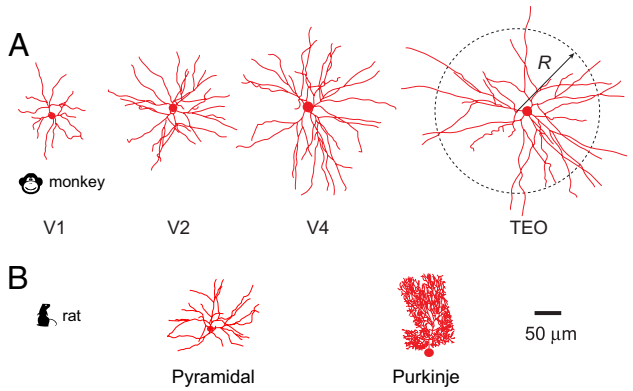

Fig. 2. Variation in dendritic arbor shape within and among different neuronal classes. (*A*) Basal dendritic arbors of pyramidal cells in different cortical areas of primates differ in total dendritic length L and arbor radius R. (*B*) Basal dendrites of a pyramidal cell are distributed more sparsely than those of a Purkinje cell. Both cells are from rat brains (refs. 26, 74, and 75, and http://NeuroMorpho.Org).

reconstructing pyramidal neurons (17, 25). Although the total dendritic length, L, and the arbor radius, R, vary widely among different areas in the neocortex, we found that they are correlated via a power law, $R \sim L^{\nu}$ (Fig. 3*A*).

Next, we explored statistical properties of branching by analyzing the spatial correlations among branches of an arbor. To this end, we counted the number of pairs of dendritic segments separated by distance r. We expressed the distance in units of R and rescaled the counts, $\tilde{n}$, so that the area under the $\tilde{n}(r/R)$ curve is normalized to 1 (Fig. 3*B*). Unexpectedly, the dependencies $\tilde{n}(r/R)$ for different arbors collapse onto a single curve (see Fig. 3*B* and *SI Appendix*, section I.3).

The universality of the pairwise correlations in the locations of dendritic segments suggests that dendritic arbors of pyramidal cells are built by statistically similar processes. Moreover, the rising part of $\tilde{n}$ is well fit by a power law $\tilde{n} \sim (r/R)^{\mu}$ (Fig. 3*B Inset*), indicating that a fragment of an arbor is statistically similar to the scaled-down version of the whole arbor (excluding the periphery) (27–32) (C. F. Stevens, personal communication). These conclusions are further supported by the fact that the measured exponent ν, characterizing the scaling of arbor dimensions across different cells (Fig. 3*A*), and the self-similarity exponent μ (Fig. 3*B*) are consistent with

$$\mu = \frac{1}{\nu} - 1, \qquad [1]$$

a relation that results from statistical similarity through a standard scaling argument (see *SI Appendix*, section I.4). Thus, we conclude that the shape of basal dendrites of pyramidal cells in the cerebral cortex exhibit universality and self-similarity.

Connectivity Repertoire and Dendritic Cost. We propose that the above statistical properties of basal dendrites of pyramidal cells can result from maximizing their functionality for a fixed dendritic cost to the organism. Let us focus first on the arbor functionality, which we identify with integrating synaptic currents from appropriate neurons. In a zeroth-order approximation, we consider which neurons synapse on the arbor rather than where the synapses are made. This approximation ignores possible nonlinear operations, which might take advantage of the synaptic location on the dendritic arbor (13–15). Yet, we think that this is a reasonable first step because nonlinear operations could not be performed if the appropriate neurons were not connected in the first place.

In an adult brain, a dendritic arbor connects with a combination of appropriate neurons, whose axons are distributed sparsely, constituting <10% of all axons passing through the arbor territory (7, 33–35). Locations of appropriate axons are not known to the dendrites before arbor growth. In the course of neuronal development, the arbor must find an appropriate combination in the ensemble of accessible neuron combinations defined by arbor dimensions. Then, finding a more appropriate combination would require choosing arbor dimensions that have a larger ensemble. Furthermore, if the developmental search strategy is sufficiently good, the larger the ensemble of neuron combinations available to the arbor, the more appropriate neuron combination can be found.

Therefore, we can quantify arbor functionality by the number of different combinations of neurons available to an arbor. To reduce the arbor functionality to an additive and extensive

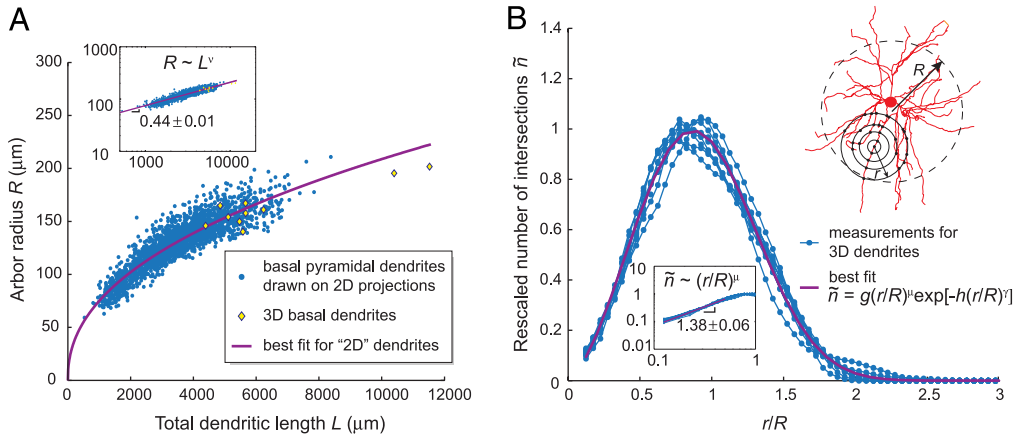

Fig. 3. Scaling, universality, and self-similarity of basal dendritic arbors of pyramidal neurons. (*A*) Dendritic arbor radius scales as a power of the total dendritic length. For 2,161 shrinkage-corrected 2D reconstructions of basal dendrites of pyramidal cells from different cortical areas, the power is 0.44 ± 0.01. The 10 available shrinkage-corrected 3D reconstructions (25) (3D dataset) are consistent with this relationship. (*Inset*) The same data on log-log scale. (*B*) Spatial pairwise correlation between dendritic segments for each neuron from the 3D dataset is shown in rescaled coordinates. (*Upper Inset*) Illustration of how the measurement was performed: counts of intersections between concentric spheres and dendritic branches were averaged over random sphere center locations in the central part of the dendritic arbor. Curves corresponding to different neurons collapse onto a master curve, fit by a universal function (magenta line), in which μ and γ are the only fitting parameters; coefficients g and h are fully determined by the normalization conditions (*SI Appendix*, section I.3). (*Lower Inset*) Shown is the rising part of the plot on log-log scale, indicating a power-law relationship and self-similarity of arbor shape.

quantity (i.e., it doubles if L is doubled), we consider the logarithm of the number of neuron combinations accessible to an arbor of given arbor dimensions, which we call the connectivity repertoire. Thus, maximizing arbor functionality reduces to finding arbor dimensions that maximize the connectivity repertoire (see *SI Appendix*, section II.1 for further details).

We computed the connectivity repertoire by adding the following 2 contributions. First, for given arbor dimensions, we counted all possible different shapes of a dendritic arbor. Each arbor shape selects a different subset of axons that pass within a spine length of a dendrite, the spine-reach zone, and, hence, can synapse on the dendrite via spine growth (Fig. 4*A*). We call the corresponding axon-dendrite proximities potential synapses (7, 36). Second, for a given arbor shape, we enumerated the number of combinations of choosing actual synapses out of potential synapses (Fig. 4*A*).

Whereas the second contribution is straightforward to calculate (7), the first contribution is challenging because locations of potential synapses are strongly correlated with each other because of the contiguous nature of an arbor. Fortunately, a similar problem has been solved in statistical physics by expressing the astronomical number of different conformations of a branched polymer in terms of its dimensions (37, 38). Using this analogy, we derived an expression for the connectivity repertoire, S, in terms of 3 arbor dimensions (see *SI Appendix*, sections II.2–5): L, R, and the average distance along the path from the tip of a branch to the cell body, ℓ (Fig. 4*A*),

$$S \simeq S_0 + \frac{L}{a}\ln(1 - R/\ell) - \frac{\ell^2}{La} - \frac{L^2}{R^2}. \qquad [2]$$

Before maximizing S in Eq. **2** with respect to R and ℓ, let us explain the biological meaning of each term. The first term contains contributions independent of R and ℓ (both from variations in arbor shape and from selecting actual synapses out of potential ones) and, thus, will not be considered further.

The second and third terms are R- and ℓ-dependent corrections to the numbers of different arbor shapes. The second term reflects the fact that straighter branches can come in fewer different shapes (38) and is always negative. As dendrites become straighter, the path length ℓ approaches from above the Euclidian distance between the tip of a branch and the cell body (approximated by R), and the second term decreases dramatically. Therefore, maximizing the number of arbor shapes favors $R \ll \ell$, that is tortuous branches (Fig. 4*B*). The third term reflects the fact that maximizing the number of arbor shapes favors branchy dendrites ($\ell \ll L$) (Fig. 4*B* and ref. 37). In these terms, a is the persistence length, below which a dendrite cannot bend (38).

The last term in Eq. **2** is an R-dependent correction to the contribution to S arising from choosing actual synapses out of potential ones. Some axons could establish more than 1 potential synapse in different locations on a dendritic arbor (Fig. 4*C*). If the entire dendritic arbor acts as a unit, differences in the locations of actual synapses from the same axon do not affect the function (39–42). As a result, additional potential synapses from the same axon are redundant and do not make a contribution to S. Thus, in calculating S, we should subtract the overcounting caused by multiple potential synapses, which, for isotropically distributed straight axons (6, 25, 43), is given by the last term.

Maximizing S favors fewer multiple potential synapses from the same axon and hence smaller last term. Reducing the last term calls for a larger R for a given L, or lower dendrite density (Fig. 4*D*). Thus, avoidance of multiple potential synapses leads to a statistical preference for arbors with sparsely distributed branches, in agreement with experimental data (see below).

However, maximization of S alone resulted in more tortuous dendrites than those observed in a pyramidal cell (see Fig. 4 *D* and *E* and *SI Appendix*, section II.6), indicating that some other factor must be responsible for the straightness of dendrites (44–46) (Fig. 4*E*). We propose that such a factor is dendritic cost minimization. Tortuous branches entail longer intracellular paths from synapses to the cell body, resulting in greater metabolic expenditures for protein transport or for counteract-

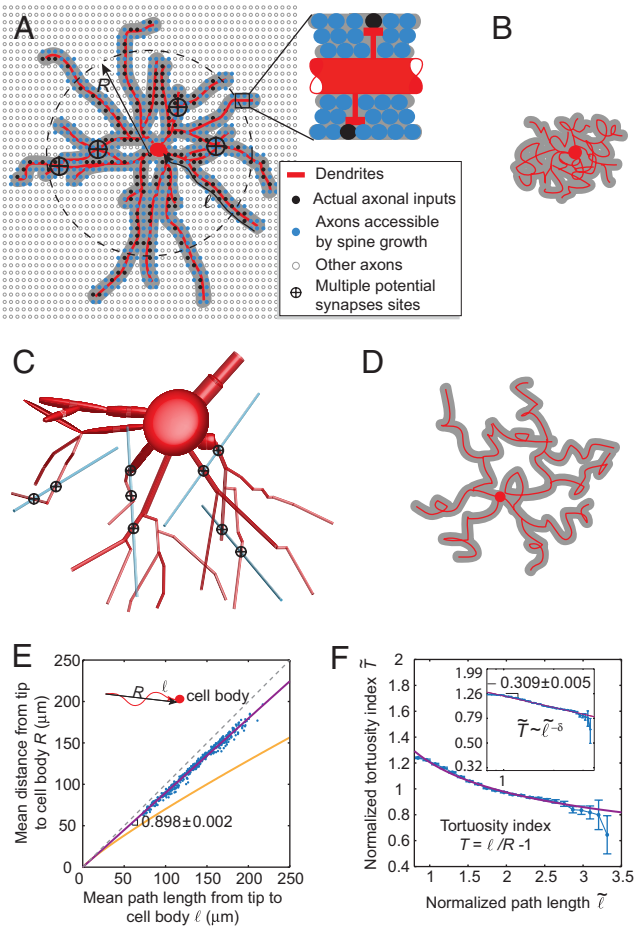

Fig. 4. Dendritic arbor shapes reflect maximization of the connectivity repertoire for a given dendritic cost. (*A*) Schematic illustration of a 3D basal dendritic arbor of pyramidal cell projected onto a plane and nearby axons that are labeled based on their relations to the arbor. For illustration purposes, we have shown all axons as running orthogonally to the plane of the drawing. Actual synapses are a subset of potential synapses, which in turn are chosen out of a larger set of axons. Potential synapses are located within the spine-reach zone of a dendrite (gray). (*B*) Tortuous and branchy dendrites maximize the total number of different arbor shapes quantified by the second and third terms in Eq. **2**. (*C*) Some axons form multiple potential synapses with a 3D dendritic arbor (crossed black circles here and in *A*). (*D*) A sparse arbor, which has lower dendrite density for a given total dendritic length, has fewer multiple potential synapses and, hence, maximizes the connectivity repertoire. (*E*) Tortuosity measured as a function of the average Euclidean distance from the tip of a branch to the cell body $R(\ell)$. The best fit (magenta line) suggests that basal dendrites are approximately straight. Orange line shows tortuous dendrites predicted from maximizing the connectivity repertoire alone, $R \sim a^{1/8}\ell^{7/8}$ (see also *D* and *SI Appendix*, section II.7 for detailed derivation). Each point represents a different cell from the 2D dataset. (*F*) Normalized tortuosity index as a function of the normalized path length from a dendritic segment to cell body. The tortuosity index T is defined as the ratio of the length along a path to the Euclidean distance between its ends minus one. In rescaled coordinates, the tortuosity was measured in units of the average index value over all paths within an arbor. The path length was measured in units of the average length over all paths within an arbor as well. Magenta line is a power law fit. *Inset* shows the same data on log-log scale. Error bars show SEM.

ing the attenuation of postsynaptic currents. By taking into account the cost contributed by path length (47–49) and total wiring length (20–23), we found that the cost function E has the scaling form $E \sim L\ell^{\delta}$ (49), where δ is model-dependent.

Predictions from Functionality-Cost Optimization and Experimental Measurements. Maximizing the connectivity repertoire for a given dendritic cost reduces to maximizing their combination: $S - \beta E$, where β is the weight of E relative to S. We solved this optimization problem (analogous to maximizing entropy for a given energy in statistical physics) and derived analytical expressions relating arbor dimensions ℓ, R, and L (see *SI Appendix*, sections II.8–10). Next, we compare these expressions with experimental measurements.

First, optimal ℓ and R satisfy the relation: $\ell/R - 1 \sim 1/\ell^{\delta}$, where $\ell/R - 1$ is defined as the tortuosity index. This prediction is consistent with measurements from basal dendrites of pyramidal cells. The tortuosity index of a path from a dendritic segment to cell body decreases with the path length and their relationship can be well fit by a power law with exponent $\delta = 0.31 +/- 0.01$ (Fig. 4*F*).

Second, our optimization framework predicts that R and L should satisfy a power law relation with the exponent $\nu = 1/(2 + \delta)$. Substituting the empirically measured value for δ, we find $\nu = 0.43$, which is not significantly different from the direct measurement of this exponent, $\nu = 0.44 +/- 0.01$ (Fig. 3*A*). In addition, by fitting the theoretical relation between R and L to measured arbor dimensions, we determined $\beta = 1.2 +/- 0.2$ $\mu m^{-1.3}$, which was unknown.

Third, the analogy between our optimization framework and the statistical physics of polymers (38) motivates the functional form of $\tilde{n}$ (Fig. 3*B*). The best-fit value of $\mu = 1.38 +/- 0.06$ (Fig. 3*B*) is not significantly different from $\mu = 1.27 +/- 0.05$, which was found by substituting the value of ν found above into Eq. **1**.

Finally, we showed that, in the case of isotropically distributed axons, avoiding multiple potential synapses leads to an arbor territory greater than the total area of the spine-reach zone (Fig. 4*A* and Fig. S3 *a* and *c* in *SI Appendix*). This accounts for the sparseness of basal dendritic arbors of pyramidal cells, which form potential synapses with only a small fraction of axons passing through the arbor territory (6) (Fig. 2*B* and Fig. S3 *a* and *c* in *SI Appendix*).

In the case of anisotropic distribution of axons and dendrites, avoidance of multiple potential synapses may not lead to a sparse arbor. For example, if all axons were oriented orthogonally to a planar dendritic arbor, such as parallel fibers and Purkinje cell dendrites in the cerebellum (50), multiple potential synapses could be avoided by arranging dendritic branches so that their spine-reach zones do not overlap. Thus, to minimize the cost of dendrites, the arbor must contract until the spine-reach zone covers most of the arbor territory, just as in Purkinje cell dendrites (49) (Fig. 2*B* and Fig. S3 *b* and *c* in *SI Appendix*). Although a projection of Purkinje dendritic arbor on the direction other than that of parallel fibers would contain many overlaps of the spine-reach zone, this would not generate multiple potential synapses for parallel fibers.

Discussion

Here, we proposed that, for a given path length cost, maximization of the connectivity repertoire, via avoiding multiple potential synapses from the same axon, accounts for statistical properties of dendritic arbors in pyramidal and Purkinje cells.

Are our results applicable to cell classes other than pyramidal and Purkinje cells? We note that the basic aspects of our theory still hold even if some assumptions were relaxed. (*i*) If presynaptic axons are tortuous and/or branchy rather than straight on the scale of a dendritic arbor, our theory would still hold but predict different scaling exponents. (*ii*) If an individual dendritic branch rather than the whole arbor acts as a unit (51–53), actual synapses from the same axon lead to the same functionality only when they occur on the same branch. In this case, calculations would be different but the general framework would still hold.

However, arbor shapes would fall outside the current theoretical framework in the following cases. (*i*) Instead of maximizing the connectivity repertoire, the objective of some dendrites could be to maximize the number of synaptic contacts with the same presynaptic neuron. One example of such scenario is photoreceptor innervation of large monopolar cells in the insect optic lobe (54). (*ii*) Spatial distribution of axons from appropriate neurons may not be a priori unknown to the arbor but partially or fully predetermined. For example, layer V apical dendrites reach out to upper cortical layers I–III containing axons of appropriate neurons, which is why we restricted our analysis to basal dendritic arbors. To determine whether our theory is applicable to various cell types, large datasets of high-quality arbor reconstructions would be desirable.

Why do we believe that the distribution of axons presynaptic to basal pyramidal dendrites is not predetermined? (*i*) Specificity in the location of pyramidal axons has been demonstrated only on the scale of cortical layers and columns, which is greater than the radius of a basal dendritic arbor ($\approx$100 μm) (55, 56). (*ii*) On the smaller scale ($<$100 μm), pyramidal axons follow relatively straight trajectories in various directions (25, 43, 46, 57–59), and, thus, are unlikely to organize into specific patterns. (*iii*) As synapses on a pyramidal dendrite are made approximately every half micrometer, it is unclear how axons from appropriate neurons could align along dendrites in such a precise manner. Even if this arrangement could be achieved for 1 dendritic arbor, thousands of other arbors present in the dendritic territory would require a rearrangement of axons from one dendrite to the next, a scenario that is highly improbable.

One may question the validity of our assumption that pyramidal cell dendrites avoid multiple potential synapses because experiments indicate that synaptically coupled cortical neurons share multiple synaptic contacts (33, 60). However, this observation does not contradict our theory for 2 reasons. First, electrophysiological recordings are heavily biased toward connected and hence nearby neurons. Although nearby neurons may make many potential synapses, these presynaptic neurons are in a minority. Indeed, in V1, 83% of synapses on a dendrite originate from neurons located farther than 200 μm in the cortical plane (61). For these presynaptic neurons, typically only 1 axonal branch courses through the dendritic arbor territory and hence is unlikely to make multiple potential synapses. Second, it is possible that various synaptic contacts form independently according to some local rules. Therefore, development can only strive to avoid multiple potential synapses but cannot guarantee their complete absence.

The cornerstone of our theory is the idea that a dendritic arbor avoids multiple hits with the same axon, which could multiply not just actual synapses, but also potential ones. Such avoidance results in a statistical repulsion between branches. To go beyond our teleological theory and speculate about possible developmental mechanisms responsible for repulsion, we must distinguish the following 2 logical possibilities. First, growing dendrites may effectively repel each other, via either extracellular or intracellular mechanism, thus making the arbor more extended and reducing multiple hits. Second, arbors somehow detect multiple hits with the same axon and rearrange their shapes in response. We think that the latter possibility is less realistic, not only because it would be difficult for a cell to detect multiple hits from the same axon on the background of simultaneous signals from thousands of other inputs, but mostly because dendrites should avoid multiplying even potential synapses that generate no electrical signal in dendrites. We therefore think that the first

possibility, avoidance of multiple hits as a consequence of interaction between branches, is more realistic.

Although a mechanism for such extracellular interaction among dendrites is unknown in vertebrates, it has been discovered in invertebrates in the form of homophilic Dscam interaction (45, 62–64). Because of a large number of stochastically chosen splice isoforms, this molecule can mediate self-repulsion among branches of the same neuron without inducing interactions among different neurons. However, Dscams are thought to be nondiffusible and hence incapable of acting over long distances. Moreover, a vertebrate homolog of invertebrate Dscam does not have a large number of splice isoforms (65, 66). We conjecture that a diffusible molecule with a large number of isoforms mediates self-repulsion in vertebrates.

Alternatively, intracellular interaction among dendrites may be reflected in arbor growth rules effectively enforcing repulsion. Historically, such growth rules have played a central role in computer simulations of arbor shapes (45, 67–69). Interestingly, effective repulsion between the cell body and dendrites was introduced to reproduce realistic arbor shapes (45). Although the proposed repulsion can explain the straightness of dendritic branches and their centripetal orientation (45, 70), it does not account for the distribution of the nearest-neighbor distance among branches (71). Here, based on the analysis of dendritic functionality, we proposed that effective repulsion exists among all segments of a dendritic arbor, not just between the cell body and dendrites.

Finally, the idea that the avoidance of multiple hits affects arbor shape may not be limited to neurons and apply to other biological objects. Consider, for example, the spatial arrangement of tree branches. As a tree strives to maximize its exposure to sunlight, its leaves must avoid shading each other (72, 73), which means that the branches should minimize multiple hits with light rays coming from the sun. Because light rays come from varying directions, they induce repulsion among branches, similarly to self-repulsion in dendritic arbors of pyramidal cells. Because the cost of branches is likely to grow with both the total length and the path length, our theory should apply to the spatial distribution of tree branches as well. Thus, the similarity of shapes between neurons and trees may not be a coincidence but arise from mathematically similar evolutionary objectives.

Methods

Arbor Reconstruction. The 2D dataset comprises 2,161 basal dendritic arbors of layer 3 pyramidal cells from primate neocortex, which were labeled in vitro with Lucifer yellow and reconstructed with a Camera Lucida by drawing on a 2D projection (17). The 3D dataset comprises 10 basal dendritic arbors of pyramidal cells from cat primary visual cortex (V1) (25), which were labeled in vivo with biocytin and reconstructed in 3D from multiple tissue sections by using Neurolucida (MicroBrightField) (www.neuromorpho.org and ref. 74). The Purkinje dataset comprises 10 Purkinje dendrites digitally reconstructed by several experimental groups (www.neuromorpho.org and refs. 75–77).

Data Analysis. We measured arbor radius and total dendritic length for Purkinje dendrites and basal pyramidal dendrites in the 2D and 3D datasets. Because cells in the 2D dataset were not digitized, we skeletonized black and white images so that dendritic segments are represented by lines 1 pixel wide. We measured pairwise correlation in the locations of dendritic segments of basal pyramidal dendrites. We also measured the tortuosity of dendrites in 345 pyramidal cells from various cortical areas of 1 vervet and 1 baboon monkey, a subset of the 2D dataset. To this end, we vectorized cell drawings by manually tracing dendrites using NeuronJ (a plug-in to ImageJ). See *SI Appendix* for further details of all measurements.

Theory. First, we derived Eq. **1** through a standard scaling argument of statistical similarity. Second, we formulated our theory based on the hypothesis that dendritic arbor shapes result from maximizing the functionality for a given dendritic cost. We argued that maximizing the dendritic functionality can be reduced to maximizing the connectivity repertoire. Third, we derived an analytical expression for the connectivity repertoire (Eq. **2**). Fourth, we derived an expression for the dendritic cost. Finally, we solved our optimization problem and compared the results with experimental measurements. See *SI Appendix* for further details of the mathematical derivation.

ACKNOWLEDGMENTS. We thank Y. Mishchenko, A. Koulakov, and M. Wyart for helpful discussions; K. Svoboda, J. Magee, L. Petreanu, T. Hu, and M. Jefferies for comments on the manuscript; and Charles Stevens for suggesting that entropy maximization could apply to dendritic arbors. Q.W. and D.B.C were supported by the Swartz Foundation and National Institutes of Health Grant MH069838. A.S. was supported by National Institutes of Health Grants NS047138 and NS063494. Part of this work was carried out at the Aspen Center for Physics (Aspen, CO).

1. Ramón y Cajal S (1899) *Texture of the Nervous System of Man and the Vertebrates* (Springer, New York).
2. Sholl DA (1953) Dendritic organization in the neurons of the visual and motor cortices of the cat. *J Anat* 87:387–406.
3. Lubke J, Roth A, Feldmeyer D, Sakmann B (2003) Morphometric analysis of the columnar innervation domain of neurons connecting layer 4 and layer 2/3 of juvenile rat barrel cortex. *Cereb Cortex* 13:1051–1063.
4. Kalisman N, Silberberg G, Markram H (2003) Deriving physical connectivity from neuronal morphology. *Biol Cybern* 88:210–218.
5. Binzegger T, Douglas RJ, Martin KA (2004) A quantitative map of the circuit of cat primary visual cortex. *J Neurosci* 24:8441–8453.
6. Braitenberg V, Schüz A (1998) *Cortex: Statistics and Geometry of Neuronal Connectivity* (Springer, Berlin), 2nd Ed.
7. Stepanyants A, Hof PR, Chklovskii DB (2002) Geometry and structural plasticity of synaptic connectivity. *Neuron* 34:275–288.
8. Stepanyants A, Chklovskii DB (2005) Neurogeometry and potential synaptic connectivity. *Trends Neurosci* 28:387–394.
9. Uttley AM (1955) The probability of neural connexions. *Proc R Soc London Ser B* 144:229–240.
10. Spruston N (2008) Pyramidal neurons: Dendritic structure and synaptic integration. *Nat Rev Neurosci* 9:206–221.
11. Fiala JC, Harris KM (1999) Dendritic structure. *Dendrites*, eds Stuart G, Spruston N, Häusser M (Oxford Univ Press, New York), 1st Ed, pp 1–34.
12. Mainen ZF, Sejnowski TJ (1996) Influence of dendritic structure on firing pattern in model neocortical neurons. *Nature* 382:363–366.
13. Haüsser M, Mel B (2003) Dendrites: Bug or feature? *Curr Opin Neurobiol* 13:372–383.
14. Poirazi P, Mel BW (2001) Impact of active dendrites and structural plasticity on the memory capacity of neural tissue. *Neuron* 29:779–796.
15. Koch C, Segev I (2000) The role of single neurons in information processing. *Nat Neurosci* 3(Suppl):1171–1177.
16. DeFelipe J, Farinas I (1992) The pyramidal neuron of the cerebral cortex: Morphological and chemical characteristics of the synaptic inputs. *Prog Neurobiol* 39:563–607.
17. Elston GN (2007) Specializations in pyramidal cell structure during primate evolution. *Evolution of Nervous Systems*, eds Kaas JH, Preuss TM (Academic, Oxford), Vol 4, pp 191–242.
18. Jacobs B, Scheibel AB (2002) Regional dendritic variation in primate cortical pyramidal cells. *Cortical Areas: Unity and Diversity*, eds Schüz A, Miller R (Taylor and Francis, London), pp 111–131.
19. Elston GN, Rosa MG (1997) The occipitoparietal pathway of the macaque monkey: Comparison of pyramidal cell morphology in layer III of functionally related cortical visual areas. *Cereb Cortex* 7:432–452.
20. Cherniak C (1992) Local optimization of neuron arbors. *Biol Cybern* 66:503–510.
21. Chen BL, Hall DH, Chklovskii DB (2006) Wiring optimization can relate neuronal structure and function. *Proc Natl Acad Sci USA* 103:4723–4728.
22. Chklovskii DB (2004) Synaptic connectivity and neuronal morphology: Two sides of the same coin. *Neuron* 43:609–617.
23. Mitchison G (1991) Neuronal branching patterns and the economy of cortical wiring. *Proc Biol Sci* 245:151–158.
24. Laughlin SB, Sejnowski TJ (2003) Communication in neuronal networks. *Science* 301:1870–1874.
25. Kisvarday ZF, Eysel UT (1992) Cellular organization of reciprocal patchy networks in layer III of cat visual cortex (area 17). *Neuroscience* 46:275–286.
26. Shepherd GM, Svoboda K (2005) Laminar and columnar organization of ascending excitatory projections to layer 2/3 pyramidal neurons in rat barrel cortex. *J Neurosci* 25:5670–5679.
27. Smith TG, Jr, Marks WB, Lange GD, Sheriff WH, Jr, Neale EA (1989) A fractal analysis of cell images. *J Neurosci Methods* 27:173–180.
28. Jelinek H, Elston GN, Zietsch B (2005) Fractal analysis: Pitfalls and revelations in neuroscience. *Fractals in Biology and Medicine*, eds Losa GA, Merlini D, Nonnenmacher TF, Weibel ER (Birkhauser, Basel), Vol 4, pp 85–94.
29. Caserta F, et al. (1990) Physical mechanisms underlying neurite outgrowth: A quantitative analysis of neuronal shape. *Phys Rev Lett* 64:95–98.
30. Rothnie P, Kabaso D, Hof PR, Henry BI, Wearne SL (2006) Functionally relevant measures of spatial complexity in neuronal dendritic arbors. *J Theor Biol* 238:505–526.
31. Jelinek HF, Fernandez E (1998) Neurons and fractals: How reliable and useful are calculations of fractal dimensions? *J Neurosci Methods* 81:9–18.

32. Milosevic NT, Ristanovic D, Stankovic JB (2005) Fractal analysis of the laminar organization of spinal cord neurons. *J Neurosci Methods* 146:198–204.
33. Markram H, Lubke J, Frotscher M, Roth A, Sakmann B (1997) Physiology and anatomy of synaptic connections between thick tufted pyramidal neurones in the developing rat neocortex. *J Physiol (London)* 500:409–440.
34. Thomson AM, Bannister AP (2003) Interlaminar connections in the neocortex. *Cereb Cortex* 13:5–14.
35. Sjostrom PJ, Turrigiano GG, Nelson SB (2001) Rate, timing, and cooperativity jointly determine cortical synaptic plasticity. *Neuron* 32:1149–1164.
36. Trachtenberg JT, et al. (2002) Long-term in vivo imaging of experience-dependent synaptic plasticity in adult cortex. *Nature* 420:788–794.
37. Gutin AM, Grosberg AY, Shakhnovich EI (1993) Polymers with annealed and quenched branchings belong to different universality classes. *Macromolecules* 26:1293–1295.
38. Rubinstein M, Colby RH (2003) *Polymer Physics* (Oxford Univ Press, New York).
39. Magee JC, Cook EP (2000) Somatic EPSP amplitude is independent of synapse location in hippocampal pyramidal neurons. *Nat Neurosci* 3:895–903.
40. Chklovskii DB, Mel BW, Svoboda K (2004) Cortical rewiring and information storage. *Nature* 431:782–788.
41. Cash S, Yuste R (1999) Linear summation of excitatory inputs by CA1 pyramidal neurons. *Neuron* 22:383–394.
42. Nevian T, Larkum ME, Polsky A, Schiller J (2007) Properties of basal dendrites of layer 5 pyramidal neurons: A direct patch-clamp recording study. *Nat Neurosci* 10:206–214.
43. Binzegger T, Douglas RJ, Martin KA (2005) Axons in cat visual cortex are topologically self-similar. *Cereb Cortex* 15:152–165.
44. Kawaguchi Y, Karube F, Kubota Y (2006) Dendritic branch typing and spine expression patterns in cortical nonpyramidal cells. *Cereb Cortex* 16:696–711.
45. Samsonovich AV, Ascoli GA (2003) Statistical morphological analysis of hippocampal principal neurons indicates cell-specific repulsion of dendrites from their own cell. *J Neurosci Res* 71:173–187.
46. Stepanyants A, Tamas G, Chklovskii DB (2004) Class-specific features of neuronal wiring. *Neuron* 43:251–259.
47. Cuntz H, Borst A, Segev I (2007) Optimization principles of dendritic structure. *Theor Biol Med Model* 4:21–28.
48. Burke RE, Marks WB (2002) Some approaches to quantitative dendritic morphology. *Computational Neuroanatomy: Principles and Methods*, ed Ascoli GA (Humana, Clifton, NJ), p 476.
49. Wen Q, Chklovskii DB (2008) A cost-benefit analysis of neuronal morphology. *J Neurophysiol* 99:2320–2328.
50. Llinás RR, Walton KD, Lang EJ (2004) Cerebellum. *The Synaptic Organization of the Brain*, ed Shepherd GM (Oxford Univ Press, New York), 5th Ed, pp 271–309.
51. Losonczy A, Magee JC (2006) Integrative properties of radial oblique dendrites in hippocampal CA1 pyramidal neurons. *Neuron* 50:291–307.
52. Poirazi P, Brannon T, Mel BW (2003) Pyramidal neuron as two-layer neural network. *Neuron* 37:989–999.
53. Poirazi P, Brannon T, Mel BW (2003) Arithmetic of subthreshold synaptic summation in a model CA1 pyramidal cell. *Neuron* 37:977–987.
54. Nicol D, Meinertzhagen IA (1982) An analysis of the number and composition of the synaptic populations formed by photoreceptors of the fly. *J Comp Neurol* 207:29–44.
55. Gilbert CD, Wiesel TN (1989) Columnar specificity of intrinsic horizontal and corticocortical connections in cat visual cortex. *J Neurosci* 9:2432–2442.
56. Mooser F, Bosking WH, Fitzpatrick D (2004) A morphological basis for orientation tuning in primary visual cortex. *Nat Neurosci* 7:872–879.
57. Fujita I, Fujita T (1996) Intrinsic connections in the macaque inferior temporal cortex. *J Comp Neurol* 368:467–486.
58. Lund JS, Yoshioka T, Levitt JB (1993) Comparison of intrinsic connectivity in different areas of macaque monkey cerebral cortex. *Cereb Cortex* 3:148–162.
59. Anderson JC, Binzegger T, Douglas RJ, Martin KA (2002) Chance or design? Some specific considerations concerning synaptic boutons in cat visual cortex. *J Neurocytol* 31:211–229.
60. Silver RA, Lubke J, Sakmann B, Feldmeyer D (2003) High-probability uniquantal transmission at excitatory synapses in barrel cortex. *Science* 302:1981–1984.
61. Stepanyants A, Martinez LM, Ferecsko AS, Kisvarday ZF (2009) The fractions of short- and long-range connections in the visual cortex. *Proc Natl Acad Sci USA* 106:3555–3560.
62. Hattori D, et al. (2007) Dscam diversity is essential for neuronal wiring and self-recognition. *Nature* 449:223–227.
63. Schmucker D, et al. (2000) *Drosophila* Dscam is an axon guidance receptor exhibiting extraordinary molecular diversity. *Cell* 101:671–684.
64. Hughes ME, et al. (2007) Homophilic Dscam interactions control complex dendrite morphogenesis. *Neuron* 54:417–427.
65. Fuerst PG, Koizumi A, Masland RH, Burgess RW (2008) Neurite arborization and mosaic spacing in the mouse retina require DSCAM. *Nature* 451:470–474.
66. Yamagata M, Sanes JR (2008) Dscam and Sidekick proteins direct lamina-specific synaptic connections in vertebrate retina. *Nature* 451:465–469.
67. Samsonovich AV, Ascoli GA (2005) Statistical determinants of dendritic morphology in hippocampal pyramidal neurons: A hidden Markov model. *Hippocampus* 15:166–183.
68. van Pelt J, Uylings HB (2002) Branching rates and growth functions in the outgrowth of dendritic branching patterns. *Network* 13:261–281.
69. Sugimura K, Shimono K, Uemura T, Mochizuki (2007) A self-organizing mechanism for development of space-filling neuronal dendrites. *PLoS Comput Biol* 3:e212.
70. Marks WB, Burke RE (2007) Simulation of motoneuron morphology in three dimensions. I. Building individual dendritic trees. *J Comp Neurol* 503:685–700.
71. Marks WB, Burke RE (2007) Simulation of motoneuron morphology in three dimensions. II. Building complete neurons. *J Comp Neurol* 503:701–716.
72. Mauseth JD (2003) *Botany: An Introduction to Plant Biology* (Jones and Bartlett, Boston), 3rd Ed.
73. Thomas PA (2001) *Trees: Their Natural History* (Cambridge Univ Press, Cambridge, UK), 1st Ed.
74. Ascoli GA (2006) Mobilizing the base of neuroscience data: The case of neuronal morphologies. *Nat Rev Neurosci* 7:318–324.
75. Martone ME, et al. (2003) The cell-centered database: A database for multiscale structural and protein localization data from light and electron microscopy. *Neuroinformatics* 1:379–395.
76. Rapp M, Segev I, Yarom Y (1994) Physiology, morphology and detailed passive models of guinea-pig cerebellar Purkinje cells. *J Physiol (London)* 474:101–118.
77. Vetter P, Roth A, Hausser M (2001) Propagation of action potentials in dendrites depends on dendritic morphology. *J Neurophysiol* 85:926–937.